Organic-silicon heterojunction solar cells: Open-circuit voltage potential and stability

Jan Schmidt, Valeriya Titova, and Dimitri Zielke

Citation: Applied Physics Letters **103**, 183901 (2013); doi: 10.1063/1.4827303
View online: http://dx.doi.org/10.1063/1.4827303
View Table of Contents: http://scitation.aip.org/content/aip/journal/apl/103/18?ver=pdfcov
Published by the AIP Publishing

Organic-silicon heterojunction solar cells: Open-circuit voltage potential and stability

Jan Schmidt,[1,2] Valeriya Titova,[1] and Dimitri Zielke[1]
[1]*Institute for Solar Energy Research Hamelin (ISFH), Am Ohrberg 1, 31860 Emmerthal, Germany*
[2]*Department of Solar Energy, Institute of Solid-State Physics, Leibniz University Hannover, Appelstrasse 2, 30167 Hanover, Germany*

(Received 19 September 2013; accepted 14 October 2013; published online 28 October 2013)

We characterize the electronic properties of crystalline silicon (c-Si)/poly(3,4-ethylenedioxythiophene): poly(styrenesulfonate) (PEDOT:PSS) junctions by means of contactless carrier lifetime measurements. The measurements demonstrate that this type of heterojunction has an unexpectedly high open-circuit voltage (V_{oc}) potential exceeding 690 mV, making it relevant for the implementation into high-efficiency c-Si solar cells. Hybrid *n*-type c-Si solar cells featuring a PEDOT:PSS hole-transport layer on the front reach an energy conversion efficiency of 12.3%. We observe a humidity-related degradation in cell efficiency during storage in air. The degradation is reduced by capping the entire device by an atomic-layer-deposited aluminum oxide film and is completely avoided in a dehumidified environment. © *2013 AIP Publishing LLC*. [http://dx.doi.org/10.1063/1.4827303]

Organic-silicon hybrid solar cells composed of an *n*-type crystalline silicon base and an organic poly(3,4-ethylenedioxythiophene):poly(styrenesulfonate) (PEDOT:PSS) hole-conducting emitter layer provide a unique possibility to combine the high energy conversion efficiencies of crystalline silicon solar cells with the potentially low fabrication cost of organic solar cells. Promising efficiencies between 8% and 12% have already been reported recently,[1–8] where the best efficiencies were realized by either passivating the organic-silicon interface using alkyl-groups[8,9] or implementing an ultrathin interface-passivating tunneling silicon oxide (SiO_x) layer between the c-Si surface and the PEDOT:PSS layer.[1,2] In this letter, we analyze the electronic properties of the c-Si/PEDOT:PSS junction by means of contactless carrier lifetime measurements to determine the potential of this junction for the application to high-efficiency c-Si solar cells. In the second part of the letter, we fabricate real devices by a simple process and characterize their electrical properties and their stability.

The electronic characterization of the silicon-organic junction is performed by measurements of the emitter saturation current density (J_{0e}) on asymmetric test structures, where the hole-conducting PEDOT:PSS layer is prepared on one side of the c-Si wafer and the other surface of the sample is passivated by silicon nitride (SiN_x). We use single-crystalline (100)-oriented 300 μm thick *p*-type float-zone (FZ) silicon wafers of 150 Ω cm resistivity. Note that since the J_{0e} measurements are performed under high-injection conditions, the conduction type of the substrate wafer is of no relevance here. After RCA cleaning of the silicon wafer, we deposit a 110 nm thick SiN_x surface-passivating layer with a refractive index of $n = 2.5$ by means of remote plasma-enhanced chemical vapor deposition (PECVD) on one side of the c-Si wafer.[10] Some c-Si wafers are then random pyramid (RP)-textured on the bare wafer side in an anisotropic KOH/iso-propanol etching solution. This is the standard texturing procedure used in c-Si solar cell production to reduce the cell's front reflection and improve its internal light trapping. In order to form a passivating tunneling layer between the organic layer and the c-Si wafer, a native oxide (SiO_x) is then grown by storing the wafer for 24 h in air. Subsequently, the samples are coated with the PEDOT:PSS precursor (F HC Solar, Clevios Heraeus GmbH) by spin-on technique at 500 revolutions per minute (rpm) for 10 s and subsequently 1000 rpm for 20 s. The samples are dried on a hotplate in air at 130 °C for 30 s. On reference samples, which were passivated with SiN_x on both surfaces, we measure the effective surface recombination velocity S_{SiN}, which is in the range between 4 and 14 cm/s in the injection range examined in this letter ($\Delta n = 10^{14}$–10^{16} cm^{-3}). Emitter saturation current densities J_{0e} are deduced from transient photoconductance decay (PCD) measurements using a WCT-120 lifetime tester from Sinton Consulting.[11] From the measured injection-dependent lifetime data we extract the emitter saturation current density J_{0e} by plotting the reciprocal effective lifetime $1/\tau_{eff}$ versus the excess carrier concentration Δn using the equation[12]

$$\frac{1}{\tau_{eff}} = \frac{1}{\tau_{intr}} + \frac{S_{SiN}}{W} + \frac{J_{0e}\Delta n}{q n_i^2 W}, \quad (1)$$

where W is the wafer thickness, q is the elementary charge, and $n_i = 8.6 \times 10^9$ cm^{-3} is the intrinsic carrier concentration of silicon at 25 °C.[13,14] As we use high-purity FZ-Si, we assume that the bulk lifetime of the c-Si samples is limited by intrinsic recombination alone, that is, Auger and radiative recombination. In Eq. (1), we use the most recent very accurate parameterization of the intrinsic lifetime of c-Si by Richter *et al.*[15] In our J_{0e} analysis, we assume that the excess carrier concentration Δn is uniform throughout the base, which is not strictly valid for large surface recombination velocities. However, for all samples measured in this study the error in J_{0e} is estimated from simulations using the device simulation tool PC1D[16] to be $\leq$25%. Due to the high substrate resistivity of 150 Ω cm (corresponding to a doping concentration of $N_{dop} = 8.9 \times 10^{13}$ cm^{-3}), all lifetime measurements in this study are performed under strict

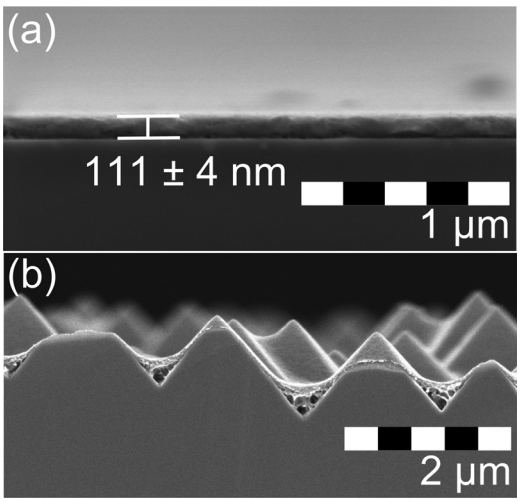

FIG. 1. SEM cross section of a PEDOT:PSS layer on (a) a planar c-Si wafer and (b) a RP-textured c-Si surface. The organic layer thickness of 111 ± 4 nm on the planar surface is laterally homogeneous, while on the RP-textured c-Si surface the valleys are partially uncovered.

high-injection conditions. Hence, it is guaranteed that Eq. (1) applies.

Figure 1(a) shows a cross-sectional scanning electron microscopy (SEM) picture of a PEDOT:PSS layer on a planar c-Si wafer surface from a high-resolution Hitachi S-4800 field emission SEM. From the SEM picture we determine the thickness of the PEDOT:PSS layer to be 111 ± 4 nm. Figure 1(b) shows an SEM micrograph of a PEDOT:PSS layer on a RP-textured c-Si surface. While the tips of the pyramids are homogeneously coated with the PEDOT:PSS layer, the valleys are partly uncovered. This problem could be solved by reducing the viscosity of the liquid precursor.

Figure 2 shows the J_{0e}-related contribution of Eq. (1) as a function of the excess carrier concentration Δn of a planar and a textured silicon sample, respectively. Using a linear fit of Eq. (1) to the measured data, we extract a surprisingly low emitter saturation current density J_{0e} of only 80 ± 3 fA/cm^2

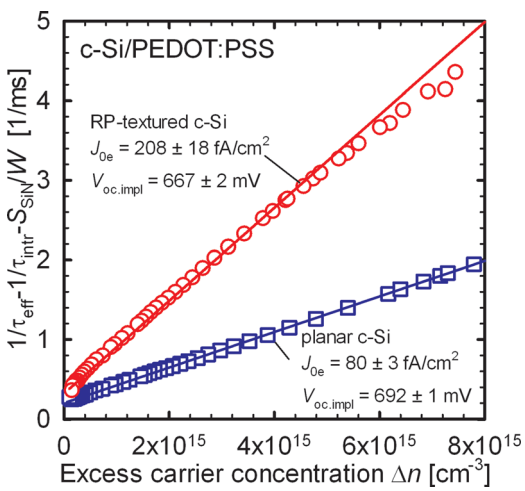

FIG. 2. Measured inverse effective lifetime $1/\tau_{eff}$ minus the inverse intrinsic lifetime $1/\tau_{intr}$ minus the surface-related lifetime S_{SiN}/W [see Eq. (1)] as a function of the excess carrier concentration Δn for a planar 150 Ω cm FZ *p*-type silicon lifetime sample (blue squares) and for a RP-textured sample (red circles). The PEDOT:PSS layer covers only one side of the wafer, the other surface is well passivated by SiN_x.

for the planar sample. Random-pyramid texturing of the silicon surface increases J_{0e} to a value of 208 ± 18 fA/cm^2. The pronounced increase in J_{0e} for the textured surface compared to the planar one can be explained by (i) the increase in the surface area by a factor 1.73 due to the pyramids and (ii) the fact that the RP-textured surface is not fully covered with the PEDOT:PSS layer, as shown by the SEM picture in Fig. 1(b). In addition to the measured J_{0e} values, we calculate the implied open-circuit voltage using the expression

$$V_{oc.impl} = \frac{kT}{q}\ln\left(\frac{J_{SC}}{J_{0e}} + 1\right), \tag{2}$$

where $kT/q = 25.69$ mV at 25 °C and a short-circuit current density J_{sc} of 40 mA/cm^2 is assumed, which is a realistic value for high-efficiency c-Si solar cells.[17] We calculate a $V_{oc.impl}$ of 692 ± 1 mV for the planar surface and a $V_{oc.impl}$ of 667 ± 2 mV for the textured surface. The planar case could be relevant for a back-junction solar cell, where the organic-silicon heterojunction is located on the planar rear side, while the front side is textured and well passivated by a transparent dielectric. Note that the V_{oc} potential determined in this study is much higher compared to the V_{oc} values realized so far on organic-silicon hybrid cells, which are mostly well below 600 mV.[3–7] Hence, organic-silicon junctions seem to have a much higher potential than commonly assumed and efficiencies in excess of 20% seem to be feasible, in particular in combination with a back-junction cell architecture.

In order to examine the applicability of our organic-silicon junctions to real devices, we fabricated solar cells using a simple process sequence. The cell structure is shown in Fig. 3. We start with a 300 μm thick phosphorus-doped (100)-oriented FZ *n*-type silicon wafer with a doping concentration of 3.2 × 10^{15} cm^{-3}. After RCA cleaning and protecting the wafer's front side with a SiN_x layer, a back surface field (BSF) is formed by phosphorus diffusion from a $POCl_3$ source in a quartz-tube furnace at 850 °C. The resulting BSF has a sheet resistance of $R_{sh.BSF} = 152 \pm 9$ Ω/sq. Next, the front SiN_x and the phosphorus silicate glass are removed in hydrofluoric acid (HF), and the wafer rear side is protected by a SiN_x protection layer. After RCA cleaning the front surface is RP-textured in a KOH/iso-propanol solution, and the SiN_x is removed by HF. A 5 μm thick aluminum layer is then

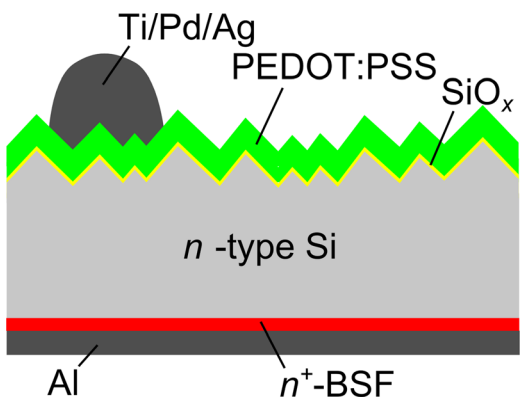

FIG. 3. Schematic of an organic-silicon hybrid solar cell on *n*-type silicon featuring a random-pyramid-textured front with a SiO_x tunneling layer and an n^+-BSF.

deposited onto the entire rear by electron beam evaporation. After rear side metallization the samples are stored in air for approximately 30 h to grow a native oxide on the front side. Subsequently, a PEDOT:PSS (Clevios F HC Solar) layer is deposited by spin-coating on the front side and dried at 130 °C for 30 s on a hotplate. The measured sheet resistance of the PEDOT:PSS layer is $R_{sh.emitter} = 172 \pm 3\,\Omega/sq$. The sheet resistance is measured using the WCT-120 tool. Finally, a titanium/palladium/silver grid is evaporated through a nickel shadow mask by electron beam evaporation. A 30 nm thick Al_2O_3 capping layer is deposited on some cells by plasma-enhanced atomic layer deposition (PA ALD) in a FlexAL (Oxford Instruments) reactor at a deposition temperature of 30 °C for encapsulating the cells.

Table I summarizes the parameters of the best solar cells of each type, measured directly after fabrication. Measurements were performed at an illumination intensity of 100 mW/cm^2 ("one sun") at a temperature of 25 °C using a commercial *IV* tester (LOANA System, pv-tools, Hamelin, Germany). All cells were measured using an aperture mask with an area of $2 \times 2\,cm^2$. Our best planar cell shows a V_{oc} of 609 mV, which is reduced to 603 mV for the RP-textured cell. The cell results are qualitatively in good agreement with the results from our J_{0e} analysis. In contrast to the J_{0e} test samples, however, our cells have a fully metalized, non-passivated rear surface which limits the V_{oc} to 614 mV.[18] This explains the overall lower V_{oc} level of the solar cells compared to our J_{0e} test structures. Further improvements in V_{oc} should hence be easily possible by passivating the solar cell rear using a dielectric layer such as SiO_2 or SiN_x. Despite their reduced V_{oc}, the highest efficiency of 12.3% was achieved on an RP-textured solar cell due to the higher short-circuit current density of 29.0 mA/cm^2 compared to a value of 27.1 mA/cm^2 for the best planar cell. Note that the general J_{sc} level of our organic-silicon hybrid devices is lower compared to standard diffused c-Si solar cells. We attribute this to parasitic light absorption in the PEDOT:PSS layer, which could be reduced by optimizing the organic precursor or by using a back-junction solar cell architecture, where no parasitic absorption takes place as the organic layer would only be deposited onto the cell rear. We have also fabricated solar cells without phosphorus-diffused BSF by just evaporating aluminum onto the bare cell rear. The best of these cells still shows an efficiency of 10.8%, but at a strongly reduced V_{oc} of only 566 mV, which is limited by the much higher recombination losses at the fully metalized solar cell rear. Also, it is well known that Al is not suitable to make a good ohmic contact to *n*-type c-Si. The relatively low fill factors measured on all fabricated cells are related to the high local ideality factors, which are in the range between 2.8 and 5.4 at maximum power point. Further detailed studies of the PEDOT:PSS/c-Si junction are required to fully understand the carrier transport and recombination via this type of heterojunction.

TABLE I. Initial parameters of the best solar cells measured at one sun (100 mW/cm^2) at a temperature of 25 °C. The aperture area of the organic-silicon cells is 4 cm^2.

Front texture	$R_{sh.BSF}$ [Ω/sq]	V_{oc} [mV]	J_{sc} [mA/cm^2]	*FF* [%]	η [%]	R_s [Ω cm^2]
Planar	152 ± 9	609	27.1	67.4	11.1	1.08
RP	152 ± 9	603	29.0	70.6	12.3	0.92
RP	No BSF	566	26.6	72.1	10.8	1.46

Figure 4 shows the measured efficiency evolution of 3 representative organic-silicon solar cells with a comparable initial efficiency of 11% during storage in darkness at room temperature. A pronounced degradation in cell efficiency is observed for the cell which is stored in air (green squares), whereas the cell which is stored in dehumidified air in a desiccator does not show any degradation (red circles). This experimental finding clearly suggests that the observed degradation is caused by the interaction of the PEDOT:PSS/c-Si junction with water molecules from the atmosphere. The inset in Fig. 4 shows how the measured illuminated current-voltage (*IV*) curves change in shape during the humidity-related degradation. A characteristic S-shaped *IV* curve forms during degradation. Because the hump in the S-shaped *IV* curve shifts to lower voltages with progressing degradation, the series resistance at maximum power point increases drastically from 1.2 to 9.1 Ω cm^2 during 1372 h of degradation and the fill factor decreases from 66.8% to 21.7%. The other strongly degrading cell parameter is the open-circuit voltage, which degrades from initially 609 to 498 mV after 1372 h. This corresponds well to J_{0e} measurements on lifetime test structures, where we measure an increase in J_{0e} by one order of magnitude within one month storage in air, which indicates a pronounced deterioration of the interface quality. Note that S-shaped *IV* curves have also been reported for other organic solar cells, where they have been attributed to the formation of interface dipoles between the PEDOT:PSS and the absorber.[19] Our degradation result might hence suggest that charges build up at the interface between the organic layer and the silicon substrate during

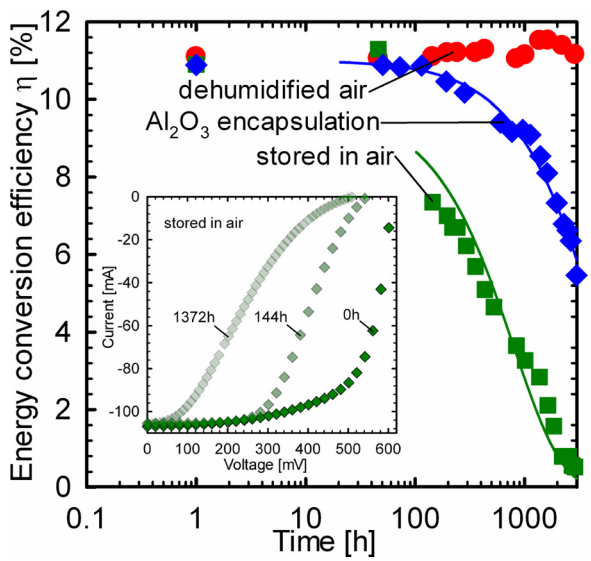

FIG. 4. Measured one-sun efficiencies of organic-silicon hybrid solar cells of comparable initial efficiency as a function of storage time in darkness. The cells are stored in air (green squares) and in a desiccator in dehumidified air (red circles). The stability is improved by encapsulating the cells with ALD-Al_2O_3 (blue diamonds). The lines are exponential fits to the measured decay curves. The inset shows the illuminated current-voltage curves during storage in air at different points in time.

interaction with water molecules. In order to improve the stability of our organic-silicon solar cells, we have encapsulated the devices with a 30 nm thick Al_2O_3 film deposited by plasma-enhanced ALD at 30 °C. ALD is known to result in highly conformal, very dense, pin-hole free layers, and Al_2O_3 deposited by ALD had already been applied for the encapsulation of organic solar cells.[20] Indeed, we observe a pronounced improvement in stability after encapsulation of our organic-silicon hybrid cells with ALD-Al_2O_3, as can be seen in Fig. 4 (blue diamonds). Exponential fits to the measured efficiency decays in Fig. 4 (lines) result in degradation time constants τ_{deg} of 794 h for the cell without encapsulation and $\tau_{deg} = 5076$ h for the encapsulated cell. This result demonstrates that the applied ALD-Al_2O_3 encapsulation is protecting the device against humidity. However, further optimization of the encapsulation layer is required to fully stabilize the organic-silicon devices.

In this letter, we have shown that the hole-conducting polymer PEDOT:PSS provides a surprisingly high level of surface passivation on c-Si wafers, as demonstrated by measured J_{0e} values of 80 fA/cm^2 on planar wafers and 208 fA/cm^2 on random-pyramid-textured c-Si surfaces. These measured J_{0e} values correspond to an implied V_{oc} of 692 mV on planar surfaces and 667 mV on textured wafers. Implementation of these layers into organic-silicon hybrid solar cells led to efficiencies up to 12.3% on 4 cm^2 aperture area and open-circuit voltages V_{oc} up to 609 mV, which were largely limited by recombination at the fully metalized cell rear. Humidity-related degradation was observed, which was significantly reduced by encapsulating the hybrid cells using atomic-layer-deposited Al_2O_3. In order to fully exploit the potential of combining organic photovoltaics with silicon-based photovoltaics, we propose to apply the organic layer to the planar rear of a c-Si wafer and implement an n^+ front surface field plus an effective dielectric passivation. Such type of organic-silicon back-junction cell would not suffer from any parasitic absorption losses in the polymer layer and could be fully metalized so that the resistive losses due to lateral current transport in the organic layer would be largely eliminated. Due to the high V_{oc} potential of the PEDOT:PSS/c-Si junction of 692 mV, such a hybrid junction would be well suited for high-efficiency solar cells.

[1]L. He, C. Jiang, H. Wang, D. Lai, and Rusli, Appl. Phys. Lett. **100**, 073503 (2012).
[2]L. He, C. Jiang, H. Wang, H. Lei, D. Lai, and Rusli, in *Proceedings of the 38th IEEE Photovoltaics Specialists Conference* (IEEE, New York, 2012), pp. 002785–002787.
[3]Q. Liu, M. Ono, Z. Tang, R. Ishikawa, K. Ueno, and H. Shirai, Appl. Phys. Lett. **100**, 183901 (2012).
[4]Q. Liu, T. Imamura, T. Hiate, I. Khatri, Z. Tang, R. Ishikawa, K. Ueno, and H. Shirai, Appl. Phys. Lett. **102**, 243902 (2013).
[5]Y. Zhu, T. Song, F. Zhang, S.-T. Lee, and B. Sun, Appl. Phys. Lett. **102**, 113504 (2013).
[6]T.-G. Chen, B.-Y. Huang, Y.-Y. Huang, E.-C. Chen, P. Yu, and H.-F. Meng, in *Proceedings of the 38th IEEE Photovoltaics Specialists Conference* (IEEE, New York, 2012), pp. 003142–003145.
[7]I. Khatri, Z. Tang, Q. Liu, R. Ishikawa, K. Ueno, and H. Shirai, Appl. Phys. Lett. **102**, 063508 (2013).
[8]Y. Zhang, F. Zu, S.-T. Lee, L. Liao, N. Zhao, and B. Sun, "Heterojunction with Organic Thin Layers on Silicon for Record Efficiency Hybrid Solar Cells," Adv. Mater. DOI: 10.1002/aenm.201300923 (published online).
[9]F. Zhang, B. Sun, T. Song, X. Zhu, and S. Lee, Chem. Mater. **23**, 2084 (2011).
[10]T. Lauinger, J. Schmidt, A. G. Aberle, and R. Hezel, Appl. Phys. Lett. **68**, 1232 (1996).
[11]R. A. Sinton and A. Cuevas, Appl. Phys. Lett. **69**, 2510 (1996).
[12]D. E. Kane and R. M. Swanson, in *Proceedings of the 18th IEEE Photovoltaics Specialists Conference* (IEEE, New York, 1985), pp. 578–583.
[13]K. Misiakos and D. Tsamakis, J. Appl. Phys. **74**, 3293 (1993).
[14]P. P. Altermatt, A. Schenk, F. Geelhaar, and G. Heiser, J. Appl. Phys. **93**, 1598 (2003).
[15]A. Richter, S. Glunz, F. Werner, J. Schmidt, and A. Cuevas, Phys. Rev. B **86**, 165202 (2012).
[16]PC1D, University of NSW, Sydney, Australia, www.pv.unsw.edu.au.
[17]D. Zielke, J. H. Petermann, F. Werner, B. Veith, R. Brendel, and J. Schmidt, Phys. Status Solidi (RRL) **5**, 298 (2011).
[18]J. Bullock, D. Yan, and A. Cuevas, Phys. Status Solidi (RRL) DOI: 10.1002/pssr.201308115 (published online).
[19]A. Kumar, S. Sista, and Y. Yang, J. Appl. Phys. **105**, 094512 (2009).
[20]K. Li, H. Fan, C. Huang, X. Hong, X. Fang, H. Li, X. Liu, C. Li, Z. Huang, and H. Zhen, Appl. Phys. Lett. **101**, 233902 (2012).